CAP/EA-ADC Method for Metastable Anions: Computational Aspects and Application to π^* Resonances of Norbornadiene and 1,4-Cyclohexadiene

Adrian L. Dempwolff, $^{1,\,\rm a)}$ Alexandra M. Belogolova, $^{2,\,3}$ Thomas Sommerfeld, $^{4,\,\rm b)}$ Alexander B. Trofimov, $^{2,\,3,\,\rm c)}$ and Andreas Dreuw $^{1,\,\rm d)}$

¹⁾ Interdisciplinary Center for Scientific Computing, Heidelberg University, Im Neuenheimer Feld 205, D-69120 Heidelberg, Germany

²⁾Laboratory of Quantum Chemistry, Irkutsk State University, Karl Marx Street 1, 664003 Irkutsk, Russia

³⁾ A. E. Favorsky Irkutsk Institute of Chemistry, Siberian Branch of the Russian Academy of Sciences, 1 Favorsky Street, 664033 Irkutsk, Russia

⁴⁾ Department of Chemistry and Physics, Southeast Louisiana University, SLU 10878, Hammond, Louisiana 70402, USA

(Dated: 19 October 2021)

The second- and third-order algebraic-diagrammatic construction schemes for the electron propagator for studies of electron attachment processes [EA-ADC(2) and EA-ADC(3)] have been extended to include the complex absorbing potential (CAP) method for the treatment of electronic resonances. Theoretical and conceptual aspects of the new CAP/EA-ADC methodology are studied in detail at the example of the well-known ${}^2\Pi_{\rm g}$ resonance of the nitrogen anion ${\rm N}_2^-$. The methodology is further applied to π^* shape resonances, for which ethylene is considered as a prototype. Furthermore, the first many-body treatment of the π_+^* and π_-^* resonances of norbornadiene and 1,4-cyclohexadiene is provided, which serve as model systems for the concept of through-space and through-bond interactions for a long time.

Keywords: electronic resonances, metastable anions, complex absorbing potentials (CAP), electronic structure theory, intermediate state representation (ISR), algebraic-diagrammatic construction (ADC), electron propagator, electron-attached states, one-electron properties

I. INTRODUCTION

During the past few years electronic resonances have been recognized as key intermediates in multiple contexts, including astrochemistry, chemical synthesis, or biology. They can be understood as discrete (N+1)-electron states with energy E_d embedded in a continuum of electronic states of an N-electron plus free-electron system. Due to the interaction with the continuum, the energy gets shifted

$$E_r = E_d + \Delta \tag{1}$$

where Δ is the shift, and E_r is the resonance position above the N-electron parent state. Moreover, the resonance is characterized by a finite lifetime τ , which is inversely related to the decay width

$$\Gamma = \frac{\hbar}{\tau}.\tag{2}$$

The two resonance parameters E_r and Γ are often combined to the complex resonance energy or Siegert energy⁷

$$E_{\rm res} = E_r - i\frac{\Gamma}{2} \tag{3}$$

as this discrete quantity is key to many theoretical analyses.

One important class of electronic resonances are shape resonances. They are metastable states possessing electronic energies above their own continua. This means that an electron may be ejected by means of a one-electron process, the released energy being transferred to the outgoing electron as kinetic energy. For this reason, shape resonances are often also referred to as open-channel resonances. Due to the one-particle nature of the decay mechanism, shape resonances are usually short-lived with typical lifetimes in the range of $\tau \sim 1$ fs, corresponding to decay widths of $\Gamma \sim 0.1$ – 1 eV.

Shape resonances occur, for example, in anionic species, and even their electronic ground state can be a resonance state. In fact, such situations are very common. Experimentally, they have been detected in many unsaturated as well as saturated organic compounds using, e.g., electron energy loss (EEL) or electron transmission spectroscopy (ETS). Besides temporary anions, shape resonances can also be encountered in highly excited or core-ionized electronic systems. ^{6,8}

One of the main difficulties encountered in the theoretical treatment of electronic resonances arises from the basis sets used by quantum chemical standard methods, which can only represent square-integrable (\mathcal{L}^2) wave functions. This condition is however not fulfilled by the sought Siegert states. Consequently, resonances can generally not be studied directly with standard quantum chemical methods: Depending on method and basis set, the lowest (or any other) state may have considerable res-

a) Electronic mail: adrian.dempwolff@iwr.uni-heidelberg.de

b) Electronic mail: thomas.sommerfeld@selu.edu

c) Electronic mail: atrof@math.isu.runnet.ru, abtrof@mail.ru

d) Electronic mail: dreuw@uni-heidelberg.de

onance character, but it is also possible that the lowest state has considerable discretized continuum character, and without any special modifications it is impossible to say how much discretized continuum character any given state possesses.

To overcome this issue, different theoretical approaches have been developed. One possibility to deal with electronic resonances in the framework of \mathcal{L}^2 -integrable quantum chemical methods is the *complex absorbing potential* (CAP) method.^{13–15} It is motivated by the fact that resonance states are characterized by discrete complex Siegert energies. These discrete states can be separated from the embedding continuum by rotating the spectrum of the Hamiltonian into the complex energy plane, ^{13,15,16} which can in principle be achieved by different means. ^{17–23}

In the CAP method, the Hamiltonian is augmented by a complex one-particle potential, thereby making all its eigenfunctions \mathcal{L}^2 -integrable.^{6,13} It has been combined with a number of electronic structure methods, among them configuration interaction (CI),^{24,25} algebraic-diagrammatic construction (ADC) for the electron propagator (also termed Dyson-ADC), 5,26,27 Fock-space coupled-cluster theory, 28 ADC for the (N-1) [or ionization potential (IP)] part of the electron propagator (IP-ADC),²⁹ symmetryadapted cluster-configuration interaction (SAC-CI),³⁰ complex density functional theory, 31 different equationof-motion coupled-cluster (EOM-CC) schemes.^{6,32,33} extended multi-configurational quasi-degenerate secondorder perturbation theory (XMCQDPT2),³⁴ extended multi-state complete active space second-order perturbation theory (XMS-CASPT2),³⁵ an electron-propagator (EP) approach based on complete active space self consistent field (CASSCF) reference states (EP-CASSCF),³⁶ and correlated independent particle Fock-space multireference coupled-cluster singles and doubles (CIP-FSMRCCSD) theory.³⁷

The CAP can in principle be added to the Hamiltonian at different stages. For the use in wave function-based methods, it can already be considered during the Hartree-Fock (HF) calculation, and this approach has been followed in the context of EOM-CC methods. 6,33 Another possibility is to include it at the post-HF stage. In ADC or CC methods, for example, a suitable basis set representation of the CAP may be added to the respective Hamiltonian before diagonalization. 6,26,27,32 In a computationally more feasible approach, the CAP is applied a posteriori, i.e., the CAP is expanded into a subspace of electronic states computed using a standard electronic structure method. The formalism has first been used in the context of CI^{25} and later also together with SAC-CI, 30 XMCQDPT2, 34 and XMS-CASPT2. 35

Recently, we introduced the new CAP/EA-ADC method, ³⁸ in which we combined the CAP subspace projection approach with ADC for the (N+1) [or electron affinity (EA)] part of the electron propagator ^{39–41} (EA-ADC) exploiting the second-order intermediate state

representation [ISR(2)] formalism. Due to the modular nature of the subspace projection approach, a combination with IP-ADC $^{39,40,42-44}$ as well as with ADC for N-electron excitations, $^{45-51}$ usually simply denoted as ADC, is straightforward and has been accomplished in Q-Chem 5.4⁵² alongside the implementation of CAP/EA-ADC. In this work, we continue our work on CAP/ADC methods. While the focus is on CAP/EA-ADC, the studied computational and conceptual aspects are equally applicable to CAP/IP-ADC and CAP/ADC.

The paper is structured as follows: after a brief review of the theoretical aspects in Section II, we present an in-depth investigation of conceptual and computational aspects of the new methodology (Sec. IV A). Then we use CAP/EA-ADC to study anionic shape resonances in the unsaturated organic molecules ethylene, norbornadiene (NBD) and 1,4-cyclohexadiene (CHD) (Sec. IV B). We finally draw conclusions in Section V.

II. THEORY

A. The Complex Absorbing Potential Method

In this section, a brief review of the CAP method is presented. A thorough mathematical analysis has been given in Ref. 13 to where the reader is referred to for further details.

Augmenting the molecular Hamiltonian with a complex one-particle potential $-i\eta \hat{W}$ leads to a complex symmetric effective Hamiltonian

$$\hat{H}(\eta) = \hat{H} - i\eta \hat{W} \tag{4}$$

with a purely discrete spectrum and \mathcal{L}^2 -integrable eigenfunctions.¹³ Therein, the parameter η is used to control the strength of the CAP. The potential function W must have a non-negative real part,

$$Re\{W(\mathbf{r})\} \geq 0$$
 and $Re\{W(\mathbf{r})\} \rightarrow \infty$ for $\mathbf{r} \rightarrow \infty$, (5)

but in general, W can be complex, in which case positive real numbers c_0 and c_1 must exist so that 13

$$|\operatorname{Im}\{W(\mathbf{r})\}| \le c_0 + c_1 \cdot \operatorname{Re}\{W(\mathbf{r})\}. \tag{6}$$

In order to rationalize how a CAP works, one may consider its effect in the time-dependent picture, where the real part of \hat{W} appears as imaginary contribution to the Hamiltonian and absorbs the outgoing electron.⁵ Any imaginary part of \hat{W} turns into an additional real potential, and can be interpreted as accelerating or slowing down the outgoing electron while it is absorbed.

In the complete basis set limit, the exact Siegert energy E_r of a resonance is recovered as $E(\eta)$ in the limit $\eta \to 0^+$. In practical applications with finite basis sets, one has to resort to a finite potential strength in order to absorb the electron within the confinement of the basis set. However, using finite η values leads to artificial reflections at the CAP boundary and by the CAP itself and

therefore to a perturbation of the resonance wave function in the bound region of the electronic system. The goal then is to find the optimal CAP strength so that the outgoing electron is effectively absorbed while the artificial reflections are minimized, i.e., to choose η as small as possible and as large as necessary.

This can be accomplished when considering a Taylor expansion of the trajectory $E(\eta)$ about $\tilde{\eta}$, a CAP strength for which the error introduced by the \mathcal{L}^2 basis set is irrelevant, 5,13

$$E(\eta) = E(\tilde{\eta}) + \sum_{n=1}^{\infty} \frac{1}{n!} \left. \frac{\mathrm{d}^n E(\eta)}{\mathrm{d} \eta^n} \right|_{\eta = \tilde{\eta}} (\eta - \tilde{\eta})^n.$$
 (7)

Evaluation of this expansion at $\eta = 0$,

$$E(0) = E(\tilde{\eta}) - \tilde{\eta} \left. \frac{\mathrm{d}E(\eta)}{\mathrm{d}\eta} \right|_{\eta = \tilde{\eta}} + \frac{1}{2} \tilde{\eta}^2 \left. \frac{\mathrm{d}^2 E(\eta)}{\mathrm{d}\eta^2} \right|_{\eta = \tilde{\eta}} + \cdots,$$
(8)

leads to a measure for the error caused by the CAP itself. Considering the *uncorrected* trajectory $E(\eta)$, this error is given by

$$|E(\eta) - E(0)| = \left| \eta \frac{dE(\eta)}{d\eta} \right| + O(\eta^2)$$

$$= \left| \frac{dE(\eta)}{d \ln \eta} \right| + O(\eta^2).$$
(9)

The best possible approximation to the exact Siegert energy is thus found for that η which minimizes the linear term in expansion (8) or, in other words, at the minimum of the logarithmic velocity of $E(\eta)$ in the complex energy plane.

Consequently, an even better approximation to the exact Siegert energy may be obtained by considering the *corrected* trajectory

$$U(\eta) = E(\eta) - \eta \frac{\mathrm{d}E(\eta)}{\mathrm{d}\eta},\tag{11}$$

for which the error to be minimized can be written as

$$|U(\eta) - E(0)| = \frac{1}{2} \left| \eta^2 \frac{\mathrm{d}^2 E(\eta)}{\mathrm{d}\eta^2} \right| + O(\eta)^3 \qquad (12)$$

$$= \frac{1}{2} \left| \eta \frac{\mathrm{d}U(\eta)}{\mathrm{d}\eta} \right| + O(\eta^3) \qquad (13)$$

$$= \frac{1}{2} \left| \frac{\mathrm{d}U(\eta)}{\mathrm{d}\ln\eta} \right| + O(\eta^3). \qquad (14)$$

Now, the best approximation to the exact Siegert energy E(0) is found at the minimum of the logarithmic velocity of $U(\eta)$. The minima of the logarithmic velocity of the corrected trajectory $E(\eta)$ and the uncorrected trajectory $U(\eta)$ [Eqs. (10) and (14)] can be located at optimal potential strengths η_{opt} by means of finite differences between eigenvalues of the effective Hamiltonian $\hat{H}(\eta)$ computed for a series of different CAP strengths η .

One may be tempted to proceed in the same way and consider even higher-order terms for the trajectory. Yet,

such a strategy does by no means guarantee more accurate results since the basis set error gets more pronounced with increasing order in Eq. (8).¹³ In practical applications, the first-order corrected trajectory (11) has proven to yield satisfactory results.^{5,33,53}

It should further be noted that results from this formalism are in principle only trustworthy in cases where the uncorrected and corrected treatments yield rather similar results.

B. Intermediate State Representation and EA-ADC

In the intermediate state representation (ISR) approach, 40,47,54 a basis of correlated excited states is constructed by letting an excitation operator \hat{C}_J act on the N-electron ground state wave function Ψ^N_0 , followed by orthogonalization,

$$\{\hat{C}_J|\Psi_0^N\rangle\} \xrightarrow{\text{Gram}} \{\tilde{\Psi}_J\}.$$
 (15)

In order to obtain an intermediate state (IS) basis suitable for computational schemes for electron attachment, \hat{C}_J is chosen such that it generates electron-attached configurations belonging to excitation classes J of one-particle (1p), two-particle-one-hole (2p-1h), ... type,

$$\{\hat{C}_J\} \equiv \{c_a^{\dagger}, c_b^{\dagger} c_a^{\dagger} c_i, c_c^{\dagger} c_b^{\dagger} c_a^{\dagger} c_i c_j, \dots\},\$$

$$a < b < c < \dots, i < j < \dots$$
(16)

Therein, c_p^{\dagger} and c_p are creation and destruction operators, respectively, associated with the HF orbital $|\varphi_p\rangle$.

To derive the EA-ADC(n) working equations, one starts from the n-th order Møller-Plesset [MP(n)] ground state wave function. Representing the molecular Hamiltonian, shifted by the respective MP(n) ground state energy E_0^N , within the resulting IS basis leads to the Hermitian ADC matrix of effective interaction \mathbf{M} whose matrix elements can be obtained as

$$M_{IJ} = \langle \tilde{\Psi}_I^{N+1} | \hat{H} - E_0^N | \tilde{\Psi}_J^{N+1} \rangle. \tag{17}$$

Similarly, the elements of the matrix of effective transition amplitudes ${\bf f}$ are given as

$$f_{Ip} = \langle \tilde{\Psi}_I^{N+1} | c_p^{\dagger} | \Psi_0^N \rangle, \tag{18}$$

and furthermore, any one-particle operator \hat{D} can be expressed in the IS basis according to

$$\widetilde{D}_{IJ} = \langle \widetilde{\Psi}_I^{N+1} | \hat{D} | \widetilde{\Psi}_J^{N+1} \rangle. \tag{19}$$

In ADC schemes, the M, f and D matrices all possess their own regular perturbative expansions and are characterized by a compact block structure as layed out, e.g., in Ref. 41. Eventually, one solves the Hermitian eigenvalue problem

$$\mathbf{MY} = \mathbf{Y}\mathbf{\Omega}, \qquad \mathbf{Y}^{\dagger}\mathbf{Y} = \mathbf{1}, \tag{20}$$

yielding electron attachment energies Ω_n as eigenvalues and the IS representation \mathbf{Y}_n of the respective electron-attached states $|\Psi_n^{N+1}\rangle$ as eigenvectors. The latter give access to the connected spectroscopic amplitudes \mathbf{x}_n according to

$$\mathbf{x}_n = \mathbf{Y}_n^{\dagger} \mathbf{f},\tag{21}$$

as well as to the transition matrix elements $T_{nm}(\hat{D})$ of a one-particle operator \hat{D} between the electron-attached states $|\Psi_n^{N+1}\rangle$ and $|\Psi_m^{N+1}\rangle$ as

$$T_{nm}(\hat{D}) \equiv \langle \Psi_n^{N+1} | \hat{D} | \Psi_m^{N+1} \rangle = \mathbf{Y}_n^{\dagger} \widetilde{\mathbf{D}} \mathbf{Y}_m.$$
 (22)

C. Combining Complex Absorbing Potentials with ADC

As mentioned above, there are different routes to introduce a CAP to electronic structure methods. In the case of ADC, the ISR formalism can be exploited to represent the CAP within the IS basis according to Eq. (19), which can then be added to the ADC Hamiltonian (17) before diagonalization. This results in a complex-symmetric diagonalization problem which, as discussed in Section II A, has to be solved repeatedly for a series of CAP strengths η .

Alternatively, the CAP may be added at the stage of converged ADC states exploiting Eq. (22). One then has to solve the complex-symmetric eigenvalue problem

$$(\mathbf{\Omega} - i\eta \mathbf{T}(\hat{W}))\mathbf{C} = \mathbf{C}\mathbf{\Omega}^c \tag{23}$$

where Ω is the diagonal matrix of (real) eigenvalues of the non-CAP-augmented ADC matrix \mathbf{M} , and $\mathbf{T}(\hat{W})$ is the transition moment matrix of the absorbing potential \hat{W} according to Eq. (22). Solving Eq. (23) yields the diagonal matrix Ω^c of complex eigenvalues of the CAP-augmented ADC Hamiltonian and the corresponding complex eigenvectors $\mathbf{C}_n = \mathbf{C}_n^{(R)} + i\mathbf{C}_n^{(I)}$, where the superscripts R and I are used to label the real and imaginary parts, respectively. The \mathbf{C}_n vectors are expansion coefficients of the CAP/ADC eigenvectors \mathbf{Y}_n^c into the eigenvector basis \mathbf{Y} of the non-CAP-augmented ADC matrix \mathbf{M} , i.e., the ISR of a CAP/ADC state can be computed according to

$$\mathbf{Y}_{n}^{c} = \mathbf{Y}\mathbf{C}_{n} = \sum_{i} C_{in}\mathbf{Y}_{i}.$$
 (24)

The motivation for this reformulation is that it allows for projection of the CAP onto a smaller subspace of electronic states. The projection method is rooted in the Weisskopf-Fano-Feshbach picture of resonances. S5-58 As discussed above, a resonance can be understood as a discrete state interacting with a continuum. As a result the resonance is mixed into the continuum, and the energy range of this mixing is determined by the width. In an \mathcal{L}^2 basis set context, the same is true, however, the mixing occurs between the resonance and pseudo-continuum states.

As a CAP separates the resonance from the continuum or pseudo-continuum, in principle, only continuum states in an energy range centered at the resonance energy with a width corresponding to at most a few resonance widths can contribute significantly to the resonance. Denoting this subspace of N_P ADC eigenstates as P, Eq. (23) is cast into

$$\mathbf{P}(\mathbf{\Omega} - i\eta \mathbf{T}(\hat{W}))\mathbf{P}\mathbf{c} = \mathbf{c}\boldsymbol{\omega}^{c}, \tag{25}$$

where **P** is the projection matrix projecting on P, and the quantities denoted by lower-case symbols, i.e., **c** and ω^c are the projected counterparts of the full-IS-space quantities **C** and Ω^c , respectively.

As both the resonance energy and width are a priori unknown, however, an approximate value for the energy can often be obtained from compact basis set calculations. Then the obvious computational protocol is to use a Davidson algorithm (or similar) to converge all states up to the estimated position as well as states in a selected—and to be converged—energy window above this position, and to execute the CAP calculation in this subspace. Still, the bulk of the final subspace spectrum consists of discretized continuum states from which the sought resonance has to be distinguished. Due to its smaller spatial extent, the latter can usually be identified as the state with the lowest $\langle \hat{r}^2 \rangle$ or, similarly, $\langle \hat{W} \rangle$ expecation value.

D. Dyson Orbitals Within CAP/EA-ADC

While it is convenient to discuss anionic shape resonances and their interactions in terms of molecular orbitals, it should be noted that the real temporary anions correspond to many-particle states that can only be approximated by a one-particle picture. However, one can retain a one-particle interpretation in a many-particle context provided Dyson orbitals are computed.

Especially in the context of electronic structure methods for electron attachment, the latter have proven to be a valuable visualization tool.⁵⁹ It has been shown⁵⁹ that the real part of a Dyson orbital of a resonance state provides a proxy for its bound part as it is largest in the valence region, while the imaginary part provides a proxy for the outgoing electron being absorbed in the CAP. We note that the bound part shows a large real and a vanishing imaginary part. In contrast, the outgoing part is represented by a complex wave with similar—but phase shifted—real and imaginary parts, and the further the wavefunction penetrates the CAP, the more its amplitude diminishes. Thus, using judicious iso-surface values, the real and imaginary parts can serve as proxies for the bound and absorption regions.

Within the projected CAP/EA-ADC approach, Dyson orbitals $|\phi_n\rangle$ can be computed according to

$$|\phi_n\rangle = \sum_p x_{pn} |\varphi_p\rangle.$$
 (26)

The needed spectroscopic amplitudes \mathbf{x}_n are computed via Eq. (21) by inserting the ISR of CAP/EA-ADC states (24), resulting in the real and imaginary parts

$$\mathbf{x}_{n}^{(R)} = \mathbf{Y}_{n}^{c(R)\dagger}\mathbf{f} = \mathbf{c}_{n}^{(R)\dagger}\mathbf{Y}^{\dagger}\mathbf{f} = \sum_{i}^{N_{P}} c_{in}^{(R)}\mathbf{Y}_{i}^{\dagger}\mathbf{f}$$
(27)

$$\mathbf{x}_{n}^{(I)} = \mathbf{Y}_{n}^{c(I)\dagger}\mathbf{f} = \mathbf{c}_{n}^{(I)\dagger}\mathbf{Y}^{\dagger}\mathbf{f} = \sum_{i}^{N_{P}} c_{in}^{(I)}\mathbf{Y}_{i}^{\dagger}\mathbf{f}.$$
 (28)

Consequently, due to the linearity of Eqs. (27) and (28) CAP/EA-ADC Dyson orbitals can be computed by linear combination of the underlying EA-ADC Dyson orbitals.

III. COMPUTATIONAL DETAILS

All results presented in this work were computed using a development version of the Q-Chem software⁵² based on version 5.2.

For the nitrogen molecule, an internuclear distance of $2.074 a_0$ was assumed. In the remaining cases, molecular geometries obtained for the neutral molecules at the MP(2)/cc-pVTZ⁶⁰ level of theory were employed throughout, being of D_{2h} symmetry in the case of ethylene and cyclohexadiene and C_{2v} symmetry in the case of norbornadiene.

In the case of N_2 , the aug-cc-pVQZ basis set^{60,61} was employed on the nitrogen atoms, and additional 3s3p3d diffuse functions were added at the molecular center. The exponents of the additional functions were: 0.0273200, 0.0136600, 0.0068300 (s); 0.0220100, 0.0110050, 0.0055025 (p); 0.0555000, 0.0277500, 0.0138750 (d). For ethylene, cyclohexadiene and norbornadiene, two different basis set combinations were used: i) cc-pVDZ⁶⁰ on hydrogen atoms and aug-cc $pVDZ^{60,61}$ on carbon atoms, with additional 4p1d diffuse functions centered at the carbon atoms, the exponents being 0.0269400, 0.0179600, 0.0119733, 0.0079822 (p) and 0.0755000 (d), denoted "DZ" throughout the remaining part of this publication; ii) cc-pVTZ⁶⁰ on hydrogen atoms and aug-cc-pVTZ^{60,61} on carbon atoms, with additional 4p1d diffuse functions centered at the carbon atoms. the exponents being 0.0237933, 0.0158622, 0.0105748, 0.0070499 (p) and 0.0400000 (d), denoted "TZ" throughout the remaining part of this paper.

In the case of third-order EA-ADC calculations, two schemes differing by the static self-energy treatment were used: i) a scheme in which the third-order static self-energy and corresponding (second-order) ground state density were used throughout (denoted as "strict" EA-ADC(3) scheme), and ii) a scheme employing the improved fourth-order static self-energy and corresponding (improved third-order) ground state density computed according to the $\Sigma(4+)$ procedure⁴⁰ (denoted as "standard" EA-ADC(3) scheme).

A smooth Voronoi CAP as first introduced in Ref. 53 was employed throughout, the functional form being de-

termined by the molecular geometry and a single onset (or cutoff) parameter r_{cut} according to

$$W(\mathbf{r}) = \begin{cases} 0 & r_{\text{WA}} \le r_{\text{cut}} \\ (r_{\text{WA}} - r_{\text{cut}})^2 & r_{\text{WA}} > r_{\text{cut}}, \end{cases}$$
(29)

with r_{WA} being a weighted-average distance according to

$$r_{\rm WA}(\mathbf{r}) = \sqrt{\frac{\sum_{\alpha} w_{\alpha} r_{\alpha}^2}{\sum_{\alpha} w_{\alpha}}}.$$
 (30)

Therein, $r_{\alpha} = \|\mathbf{r}_{\alpha}\| = \|\mathbf{r} - \mathbf{R}_{\alpha}\|$ is the distance between \mathbf{r} and the coordinates \mathbf{R}_{α} of atom α , and the summations are carried out over all atoms α . The weight parameter w_{α} is given as

$$w_{\alpha} = \frac{1}{\left(r_{\alpha}^2 - r_{\text{nearest}}^2 + (1 \text{ a.u.})^2\right)^2},$$
 (31)

with $r_{\text{nearest}} = \|\mathbf{r}_{\text{nearest}}\| = \|\mathbf{r} - \mathbf{R}_{\text{nearest}}\|$ being the distance between \mathbf{r} and the atom closest to this point in space. For all calculations presented in this work, an onset of $r_{\text{cut}} = 3.5 \, a_0$ was used, and the basis set representation of $W(\mathbf{r})$ was computed by numerical quadrature on a grid consisting of 974 Lebedev angular and 250 Euler-MacLaurin radial points as implemented in Q-CHEM 5.2.

For the CAP representation $\mathbf{T}(\hat{W})$ within a given subspace of converged EA-ADC eigenstates, the second-order intermediate state representation [ISR(2)] formalism was used. The number of EA-ADC vectors with lowest eigenvalues included within the CAP calculations were: 30 (ethylene anion $^2\mathrm{B}_{2\mathrm{g}}$ resonance), 30 (cyclohexadiene anion $^2\mathrm{A}_{\mathrm{u}}$ and $^2\mathrm{B}_{2\mathrm{g}}$ resonances), 50 (norbornadiene anion $^2\mathrm{A}_{2}$ resonance) and 30 (norbornadiene anion $^2\mathrm{B}_{2}$ resonance). If not stated otherwise, in case of the $^2\mathrm{H}_{\mathrm{g}}$ resonance of the dinitrogen anion the number of subspace vectors included was 200 for all considererd EA-ADC schemes. For each investigated resonance state, the considered subspace consisted exclusively of vectors transforming according to the same irreducible representation within the largest Abelian subgroup of the molecular point group of symmetry.

If not explicitly specified otherwise, trajectories were computed for real potential strengths η , and resonance parameters were extracted from the corrected trajectories according to Eq. (11) at the minimum of the respective logarithmic velocity (14). In case of the 2A_2 resonance of the norbornadiene anion, the assignment of the stabilization point was further supported by considering a series of molecular geometries along the ring puckering coordinate (see supplementary material for further details).

Finally, Dyson orbital plots were generated using version 1.9.4a27 of the VMD software, 62 employing input data obtained by linear combination of Dyson orbitals computed for EA-ADC(2)/TZ eigenstates of the respective non-CAP-augmented EA-ADC Hamiltonians as outlined in Section II D.

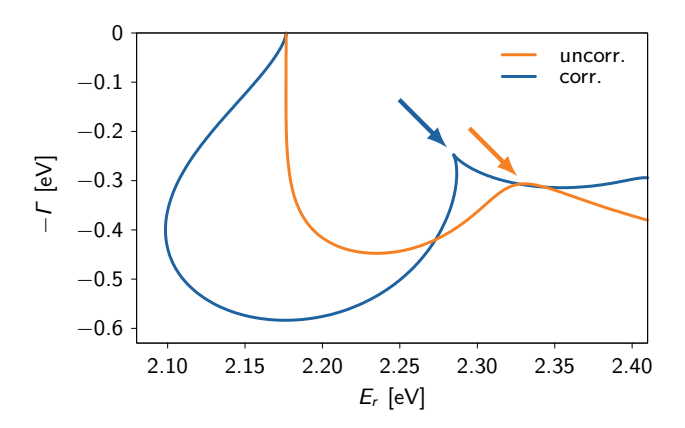


FIG. 1. Corrected (blue) and uncorrected (orange) complex energy trajectories for the $^2\Pi_{\rm g}$ resonance of the dinitrogen anion computed using standard EA-ADC(3). The resonance positions are marked with arrows.

IV. RESULTS AND DISCUSSION

The newly developed CAP/EA-ADC methodology was applied for the computational description of a number of π^* shape resonance states. As a first test, different methodological aspects were investigated at the example of the well-studied $^2\Pi_{\rm g}$ resonance state of the dinitrogen anion ${\rm N}_2^-$ (Sec. IV A). The applicability of the method was further evaluated in a study of π^* resonances in unsaturated hydrocarbons: ethylene (Sec. IV B 1), norbornadiene, and 1,4-cyclohexadiene (Sec. IV B 2). The diene molecules are of particular interest because the properties of their π^* resonance states can be directly interpreted by means of the concept of through-bond and through-space interactions, which has been an active field of research for a long time. 63,64

A. A First Test: $^2\Pi_{\rm g}$ Resonance of the Dinitrogen Anion

The first example studied using the newly developed methodology needs to be a well understood resonance for which reliable reference data are available. For this purpose, we use the ${}^2\Pi_{\rm g}$ resonance of ${\rm N}_2^-$, which has been subject of extensive studies in the past decades. A compilation of resonance positions and widths computed using a variety of theoretical approaches can be found in Ref. 65. The most accurate value so far was obtained analyzing experimental cross sections with a Feshbach projection formalism based on experimental data. 66 In this study, a resonance position of $E_r = 2.32$ eV and a width of $\Gamma = 0.41$ eV was found, and these values have been used as a reference since then.

The corrected and uncorrected trajectories computed using standard CAP/EA-ADC(3) are depicted in Figure 1. At the minimum of the logarithmic velocity, a resonance position of $E_r = 2.327$ eV and a decay width of $\Gamma = 0.307$ eV are obtained from the uncorrected

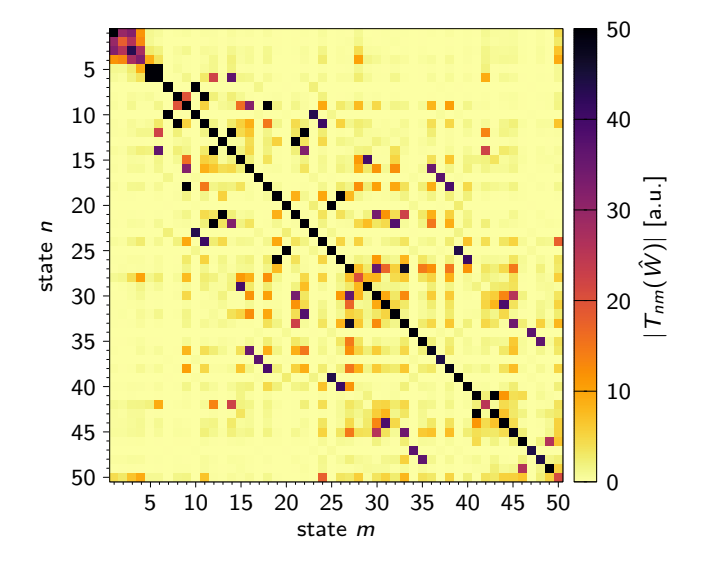


FIG. 2. Transition matrix $\mathbf{T}(\hat{W})$ of a smooth Voronoi potential in the subspace of the 50 energetically lowest standard EA-ADC(3) states of N_2 , ordered by their respective energies. The best approximation to the $^2\Pi_{\rm g}$ resonance is provided by state 2. Direct coupling to this state, indicated by non-zero off-diagonal elements, is mainly observed within the subspace of the four lowest states.

trajectory. Using the corrected trajectory, similar values are found, the resonance position and width being $E_r=2.285$ eV and $\Gamma=0.247$ eV, respectively. Thus, both the uncorrected and corrected treatment yield resonance positions which are in excellent agreement with the reference value. In case of the resonance width, the value extracted from the uncorrected trajectory lies somewhat closer to the reference than the corrected one. However, when compared to other theoretical approaches, both computed widths lie well within the usual range of variation. As an example, one may consider a corresponding CAP/EOM-EA-CCSD study, where a similar behavior was observed for the corrected and uncorrected resonance widths, which were found to be $\Gamma=0.364$ eV and $\Gamma=0.286$ eV, respectively.

1. Choice of the Subspace

After this encouraging result, the problem of the choice of the subspace of EA-ADC states used for the CAP representation was addressed. As discussed in Sec. II C, the Weisskopf-Fano-Feshbach picture of resonances implies that only states close to the position of the resonance in question can be expected to significantly contribute to its description. Figure 2 displays the representation of a smooth Voronoi potential within the subspace of 50 states at the lower end of the standard EA-ADC(3) spectrum of N_2 as computed according to Eq. (22). Therein, dark diagonal elements indicate diffuse pseudo-continuum states, which exhibit a strong interac-

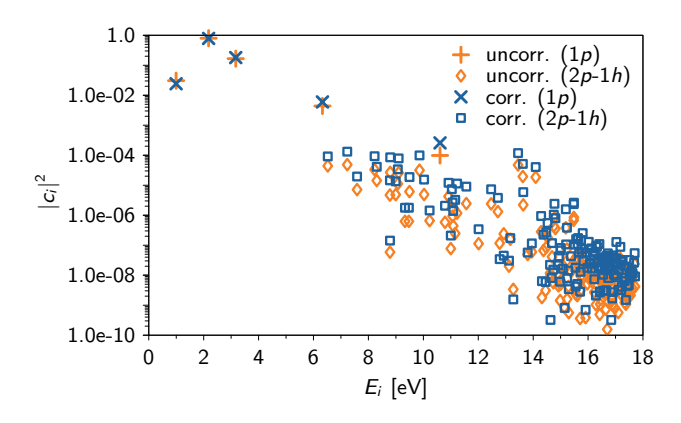


FIG. 3. Overlaps $|c_i|^2$ of EA-ADC states \mathbf{Y}_i with the $N_2^{-2}\Pi_g$ resonance as computed in the subspace of 200 standard EA-ADC(3) eigenstates of energy E_i at the uncorrected (orange) and corrected (blue) complex energy velocity minimum. The individual states are distinguished as one-particle $(1p, \text{ pole strength} \geq 0.5)$ and two-particle-one-hole states $(2p\text{-}1h, \text{ pole strength}} < 0.5)$.

tion with the (diffuse) potential. Light diagonal elements, on the other hand, are associated with more compact resonance states, and indeed, the energetically second-lowest state (state 2 in Fig. 2) turns out to have the largest overlap with the $^2\Pi_{\rm g}$ resonance of N_2^- .

One can now estimate which states will have the strongest effect on the resonance upon addition of the CAP by considering the direct couplings, i.e., the off-diagonal elements belonging to this state. Inspection of Figure 2 shows that such couplings mainly exist with states close in energy, i.e., states 1, 3 and 4, which should consequently be included in the subspace. However, additional states could still be involved by means of indirect or weak direct coupling.

Another perspective on the selected subspace can be gained from considering the resonance vector in the largest considered subspace of 200 standard EA-ADC(3) states of N_2 . Figure 3 shows a plot of the overlaps $|c_i|^2$ between the resonance at the stabilization point and EA-ADC states \mathbf{Y}_i against the respective state energies E_i . As already pointed out in the context of projected CAP/CI,²⁵ the distribution roughly matches a Breit-Wigner profile. It is thus evident that mainly EA-ADC(3) states in the energetic vicinity of the resonance position need to be included in the subspace. Another conclusion which can be drawn from Fig. 3 is that main (1p) states are generally more important for the description of the resonance than satellite (2p-1h) states.

Finally, the subspace quality can be assessed by means of the convergence of the resonance parameters. For this purpose, trajectories were computed for increasing subspace sizes (Figure 4). For small potential strengths, resulting in computed widths Γ close to zero, barely any difference can be observed between the different trajectories. The variations get more pronounced for stronger potentials, i.e., at the right edge of Figure 4. In this sys-

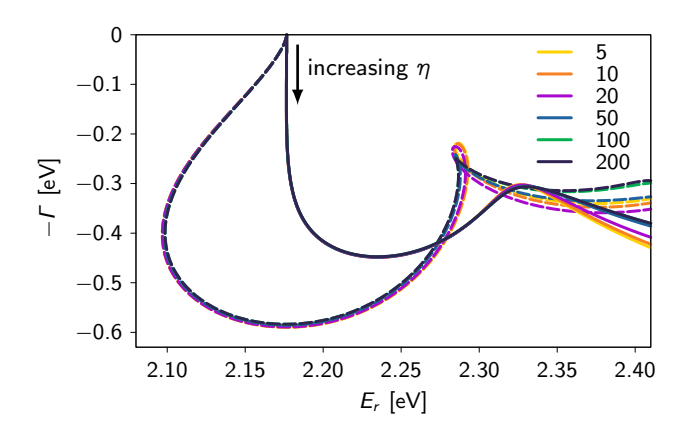


FIG. 4. Corrected (dashed) and uncorrected (solid) standard CAP/EA-ADC(3) resonance energy trajectories of the $^2\Pi_{\rm g}$ resonance of N $_2^-$ computed using different subspace sizes between 5 and 200.

tem, larger deviations are seen only beyond the stabilization point. The resonance parameters extracted from the corrected and uncorrected trajectories are summarized in Table I along with the sum of overlaps $|c_i|^2$ for each considered subspace size, evaluated using the c_i coefficients obtained for the largest subspace of 200 EA-ADC(3) vectors at the respective stabilization point $\eta_{\rm opt}$.

As already implied by Figure 4, nearly no difference is observed between the smallest and largest subspace considered in case of the uncorrected treatment. For the corrected treatment, a more pronounced shift towards larger decay widths is observed when increasing the subspace size used for the CAP representation. However, the difference between the decay widths computed using subspace sizes of 5 and 200 is still only 0.03 eV. The resonance position, on the other hand, is nearly unaffected. The faster convergence of the uncorrected resonance parameters is also reflected in a faster convergence of the sum of overlaps $|c_i|^2$.

2. The Effect of Different EA-ADC Approximation Schemes

So far only the standard EA-ADC(3) scheme has been considered. In this section, we examine the performance of different EA-ADC schemes. Figure 5 displays the corrected (dashed) and uncorrected (solid) trajectories computed using standard and strict EA-ADC(3) as well as EA-ADC(2). The resonance parameters extracted from the respective trajectories are summarized in Table II.

In comparison with standard EA-ADC(3), the strict EA-ADC(3) scheme yields resonance widths closer to the reference value of $\Gamma=0.41~\rm eV$. ⁶⁶ At the same time, larger errors of 0.10 eV and 0.15 eV are found for the corrected and uncorrected resonance positions, respectively. Most notably, the level of accuracy found for EA-ADC(2) is comparable to that of standard EA-ADC(3). Especially

TABLE I. Standard CAP/EA-ADC(3) resonance parameters of the $N_2^{-2}\Pi_g$ resonance extracted from the uncorrected and corrected trajectories for different subspace sizes. The quality of the subspace with respect to the largest considered subspace of 200 EA-ADC(3) vectors may be judged by means of the sum of overlaps $|c_i|^2$.

subspace size	Uncorrected				Corrected				
N_P	$E_r [eV]$	$\Gamma [\mathrm{eV}]$	$\eta_{ m opt}$	$\sum_{i}^{N_P} c_i ^{2 \text{ a}}$	$E_r [eV]$	$\Gamma [eV]$	$\eta_{ m opt}$	$\sum_{i}^{N_P} c_i ^{2 \text{ a}}$	
5	2.325	0.302	2.77×10^{-3}	0.999571	2.286	0.218	5.57×10^{-3}	0.998796	
10	2.326	0.303	2.77×10^{-3}	0.999660	2.286	0.220	5.53×10^{-3}	0.999041	
20	2.326	0.303	2.76×10^{-3}	0.999749	2.284	0.225	5.39×10^{-3}	0.999311	
50	2.327	0.306	2.71×10^{-3}	0.999954	2.284	0.242	5.11×10^{-3}	0.999885	
100	2.327	0.307	2.69×10^{-3}	0.999999	2.285	0.247	4.99×10^{-3}	0.999997	
200	2.327	0.307	2.69×10^{-3}	1.000000	2.285	0.247	4.99×10^{-3}	1.000000	

^a Evaluated using c_i coefficients obtained for subspace size 200 at the respective stabilization point.

TABLE II. Resonance parameters of the $N_2^{-2}\Pi_g$ resonance extracted from the uncorrected and corrected trajectories computed using different EA-ADC schemes.

		Uncorrecte	ed		Corrected	i
EA-ADC scheme	$E_r [eV]$	$\Gamma \left[\mathrm{eV} \right]$	$\eta_{ m opt}$	$E_r [eV]$	$\Gamma \left[\mathrm{eV} \right]$	$\eta_{ m opt}$
$\overline{\text{EA-ADC}(2)}$	2.354	0.303	2.83×10^{-3}	2.310	0.260	4.96×10^{-3}
Strict EA-ADC(3)	2.471	0.350	2.74×10^{-3}	2.422	0.290	5.03×10^{-3}
Standard EA-ADC(3)	2.327	0.307	2.69×10^{-3}	2.285	0.247	4.99×10^{-3}

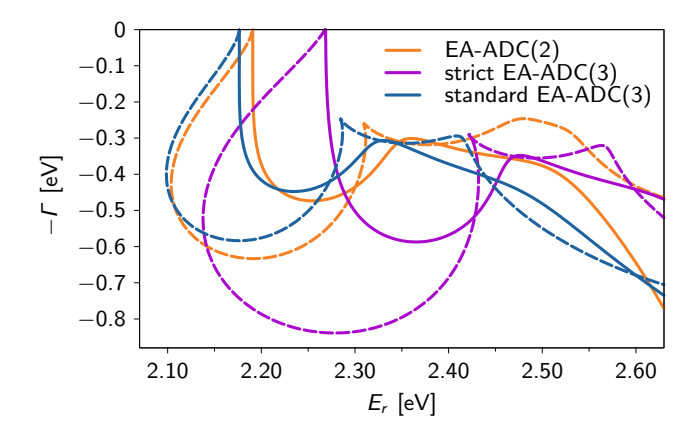


FIG. 5. Corrected (dashed) and uncorrected (solid) resonance energy trajectories of the dinitrogen anion $^2\Pi_{\rm g}$ resonance computed using different EA-ADC schemes.

the resonance position obtained from the corrected trajectory ($E_r = 2.31 \text{ eV}$) is in excellent agreement with the reference value of $E_r = 2.32 \text{ eV}$, showing an error of only 0.01 eV. While the good performance of the second-order scheme might seem surprising, it comes not totally unexpected. As is evident from Fig. 3, the description of shape resonances mainly builds upon the accurate description of one-particle states, which, as we have recently shown, 41 can be provided by EA-ADC(2).

3. Extension to Complex Potential Strengths

Within the projected CAP approach, it is straightforward to extend the methodology to complex potential strengths $\eta = |\eta| (\cos \vartheta + i \sin \vartheta)$, since only minor modifications of the η -trajectory-generating code are required. Here, an approach similar to that introduced in the context of CAP/XMCQDPT2³⁴ has been followed.

As discussed in Section IIA, the logarithmic velocity of the (uncorrected or corrected) complex energy of a resonance state with respect to the potential strength parameter can be considered a metric for the quality of the approximation [cf. Eqs. (10) and (14)]. Figure 6 displays plots of these quantities for a section of the two-dimensional $\left\{ \left|\eta\right| ,\vartheta\right\}$ parameter space as computed in the subspace spanned by 200 standard EA-ADC(3) eigenstates. Therein, minima correspond to the best approximations of the uncorrected and corrected complex energy $E(\eta)$ and $U(\eta)$, respectively, with respect to the exact Siegert energy E(0). The global velocity minimum for the corrected energy [Figure 6 b)] is found at virtually the same position as in the case of real potential strengths. It is located at $(\left|\eta\right|_{\mathrm{opt}},\vartheta_{\mathrm{opt}}) =$ $(4.99 \times 10^{-3}, -0.1^{\circ})$, for which the resonance position and width are $E_r = 2.285$ eV and $\Gamma = 0.247$ eV. In the uncorrected case [Figure 6 a)], the global minimum is found at $(|\eta|_{\text{opt}}, \vartheta_{\text{opt}}) = (2.66 \times 10^{-3}, -16.1^{\circ})$. However, nearly no improvement of the resonance parameters over those computed with a purely real potential strength is observed. The resonance position of $E_r = 2.328 \text{ eV}$ is virtually unaffected, and also the resonance width of $\Gamma = 0.321 \text{ eV}$ is only slightly shifted towards the reference value of $\Gamma = 0.41 \text{ eV}.^{66}$ Another observation is

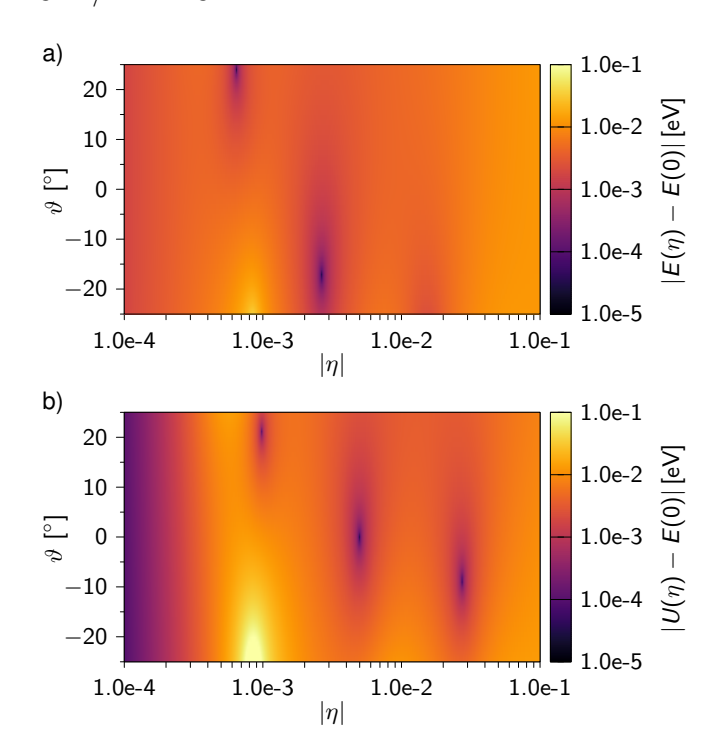


FIG. 6. Logarithmic velocity of the a) uncorrected trajectory $|E(\eta)-E(0)|$ [cf. Eq. (10)] and b) corrected trajectory $|U(\eta)-E(0)|$ [cf. Eq. (14)] of the $^2\Pi_{\rm g}$ resonance of N $_2^-$ evaluated for complex potential strengths $\eta=|\eta|$ (cos $\vartheta+i\sin\vartheta$). A subspace of 200 standard EA-ADC(3) states was used.

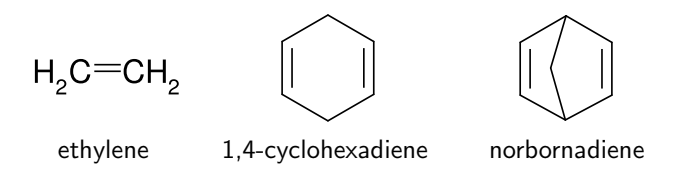


FIG. 7. Molecular structures of unsaturated hydrocarbons considered in this study.

that the stabilization point of the uncorrected trajectory computed for different angles $\vartheta \lesssim 10^{\circ}$ is found at very similar potential strengths $|\eta|$, reflected in a nearly perfectly vertical "valley" in Figure 6 a) at $|\eta| \approx 2.7 \times 10^{-3}$.

Combining these findings, additional accuracy may be gained by going to complex potential strengths. However, the treatment using real potential strengths (and thus, a purely imaginary CAP) yields similarly accurate results, and therefore this methodology will be used throughout the remaining part of this study.

B. π^* Resonances in Unsaturated Hydrocarbons

Temporary anion π^* resonances have been commonly observed in many unsaturated organic molecules.^{9,11} Much experimental and theoretical work has been devoted to these molecules as the π^* resonances character-

ize the lowest unoccupied "orbitals" and provide therefore a proxy for the electron acceptor properties of these compounds in donor/acceptor reactions.

1. Ethylene

The prototype for unsaturated hydrocarbons is ethylene (Fig. 7), for which a π^* shape resonance of B_{2g} symmetry has been experimentally identified.^{9,67} In these studies, the resonance position was determined at $E_r = 1.78 \text{ eV}$ in ETS experiments⁹ and later at $E_r \approx 1.8 \text{ eV}$ by elastic electron scattering (ES).⁶⁷ In the latter work, the width of this resonance was determined as $\Gamma = 0.7 \text{ eV}$.

A compilation of the various available theoretical resonance parameters is given in Ref. 65. Most notably, CAP/EOM-EA-CCSD calculations yielded a resonance position of $E_r=2.091$ eV using the corrected trajectory, while the corresponding decay width is given as $\Gamma=0.430$ eV.⁶⁵

Table III summarizes the results obtained using CAP/EA-ADC. As it has already been observed for the $^2\Pi_{\rm g}$ resonance of N $_2^-$, EA-ADC(2) performs extraordinarily well with respect to the resonance position. The value obtained using the triple-zeta basis set agrees perfectly with the experimental value of $E_r=1.80$ eV. The resonance width, on the other hand, seems to be better reproduced by the EA-ADC(3) treatment, where the differences between strict and standard EA-ADC(3) are generally not as pronounced as in the case of N $_2^-$.

2. Dienes: 1,4-Cyclohexadiene and Norbornadiene

In the past decades, there has been a long-standing discussion among physical organic and theoretical chemists, as to whether the interactions between ethylenic π -orbitals of cyclic diene molecules may lead to a "reversal" of the *natural* energetic order of the resulting molecular orbitals. In this context, the concept of *through-space* and *through-bond* interactions was introduced.⁶⁴

If the molecular system lacks any additional orbitals that couple with the π -system, the π -type molecular orbitals can simply be constructed from suitable linear combinations of the ethylenic π orbitals, that is, the π and π^* orbitals associated with every double bond. This case is referred to as through-space interaction and results in a natural energetic ordering of the π -type molecular orbitals. An example is norbornadiene (Fig. 7), where the two unoccupied π^* molecular orbitals can be constructed from the ethylenic π^* orbitals of the two double bonds: The symmetric "+"-combination π^*_+ minimizes the number of nodal planes and consequently has a lower orbital energy than the antisymmetric "–"-combination π^*_- .

An example for a *through-bond* interaction is provided by 1,4-cyclohexadiene (Fig. 7). Since the carbon skeleton is planar, additional orbitals of π compatible symmetry

TABLE III. Resonance parameters of the ethylene ² B _{2g} resonance as extracted from the corrected trajectory computed using
different EA-ADC schemes and employing double-zeta (DZ) and triple-zeta (TZ) basis sets as specified in Section III.

		DZ				TZ			
EA-ADC scheme	$E_r [eV]$	$\Gamma \left[\mathrm{eV} \right]$	$\eta_{ m opt}$	-	$E_r [eV]$	$\Gamma\left[\mathrm{eV}\right]$	$\eta_{ m opt}$		
EA-ADC(2)	2.029	0.434	4.27×10^{-3}		1.802	0.353	2.94×10^{-3}		
Strict EA-ADC(3)	2.154	0.538	4.28×10^{-3}		2.048	0.547	2.99×10^{-3}		
Standard EA-ADC(3)	2.097	0.493	4.25×10^{-3}		1.971	0.478	2.97×10^{-3}		

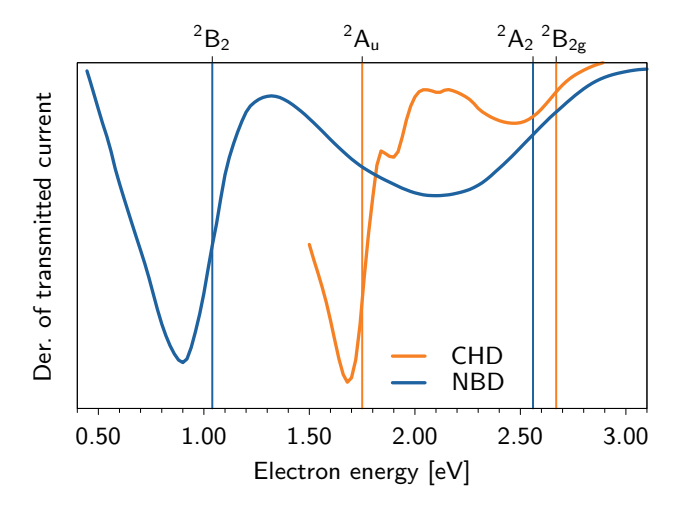


FIG. 8. Electron transmission spectra recorded for norbornadiene (NBD, blue) and 1,4-cyclohexadiene (CHD, orange). Experimentally determined resonance energies are indicated by vertical lines. Data digitized from Ref. 68.

can be constructed by linear combination of the four C-H σ orbitals of the methylene moieties. In particular, the occupied σ orbital combination of appropriate symmetry will interact with the π_+^* orbital resulting in a stabilized occupied and a destabilized unoccupied combination, and by this means the π_+^* orbital will be pushed energetically above the unaffected π_-^* orbital.

As ethylene, both 1,4-cyclohexadiene and norbornadiene, cannot bind excess electrons in their unoccupied π^* molecular orbitals, and all electron-attached states are temporary anions or resonances. Experimentally, these anions have been identified by ETS,⁶⁸ and eventually assigned using high-energy electron impact measurements⁶⁹ and comparative ETS studies of 1,4-dioxane and similar molecular systems.⁷⁰ The recorded electron transmission spectra of both diene molecules are displayed in Figure 8.⁶⁸

According to these studies, the $^2\mathrm{B}_{2\mathrm{g}}$ resonance of the 1,4-cyclohexadiene anion (π_+^* combination) is indeed found at a higher energy ($E_r = 2.67$ eV) than the $^2\mathrm{A}_\mathrm{u}$ state (π_-^* combination) which shows a resonance position of $E_r = 1.75$ eV. In contrast, for norbornadiene the normal ordering is preserved: The $^2\mathrm{B}_2$ resonance (π_+^* combination) is observed at lower energy ($E_r = 1.04$ eV) than the $^2\mathrm{A}_2$ resonance (π_-^* combination), for which the resonance position was determined as $E_r = 2.56$ eV. How-

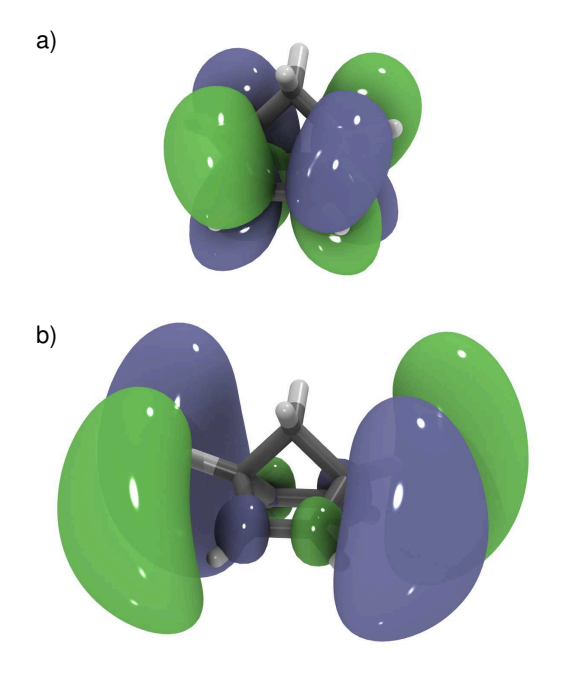


FIG. 9. a) Real and b) imaginary parts of the normalized Dyson orbital corresponding to the 2A_2 (π_-^*) shape resonance of the norbornadiene anion computed at the EA-ADC(2)/TZ level of theory. Isosurfaces were drawn at function values of ± 0.016 (real part) and ± 0.011 (imaginary part).

ever, owing to the lack of vibrational resolution in the electron transmission spectra, no direct conclusion can be drawn about the widths of these states.

On the theoretical side, a number of studies have been conducted, most notably using the stabilization technique combined with Koopmans' theorem and a multi-reference CIS approach geared towards recovering orbital relaxation, but no electron correlation. ^{71,72} These stabilization calculations confirm the reversal of the energetic ordering of the π^* orbitals in 1,4-cyclohexadiene. Here, we study these resonances for the first time at the many-particle level.

We start with norbornadiene. The real parts of the normalized Dyson orbitals of the 2A_2 and 2B_2 resonance states of norbornadiene as calculated at the CAP/EA-ADC(2)/TZ level of theory are displayed in Figures 9 and 10, respectively. The weights of the Dyson orbitals of 0.954 (2A_2) and 0.926 (2B_2) thereby indicate considerable one-electron character of the respective attachment processes, the relative weights of the real/imaginary parts

TABLE IV. Resonance parameters of the 2B_2 and 2A_2 anionic shape resonances of norbornadiene as extracted from the corrected trajectories computed using different EA-ADC schemes and employing double-zeta (DZ) and triple-zeta (TZ) basis sets as specified in Section III. The experimentally determined resonance positions are $E_r(^2B_2) = 1.04$ eV and $E_r(^2A_2) = 2.56$ eV.

		DZ				TZ			
State	EA-ADC scheme	$E_r [eV]$	$\Gamma \left[\mathrm{eV} \right]$	$\eta_{ m opt}$	$E_r [eV]$	$\Gamma [eV]$	$\eta_{ m opt}$		
$^{2}\mathrm{B}_{2}~(\pi_{+}^{*})$	EA-ADC(2)	1.185	0.217	2.41×10^{-3}	0.955	0.189	6.64×10^{-4}		
	Strict EA-ADC (3)	1.577	0.380	1.52×10^{-3}	1.564	0.410	1.08×10^{-3}		
	Standard EA-ADC (3)	1.563	0.362	1.51×10^{-3}	1.495	0.351	1.06×10^{-3}		
$^{2}A_{2} (\pi_{-}^{*})$	EA-ADC(2)	2.905	1.103	4.25×10^{-3}	2.586	0.955	2.42×10^{-3}		
	Strict EA-ADC (3)	3.647	1.192	1.08×10^{-2}	3.375	0.983	6.69×10^{-3}		
	Standard EA-ADC(3)	3.626	1.186	1.06×10^{-2}	3.310	0.944	6.39×10^{-3}		

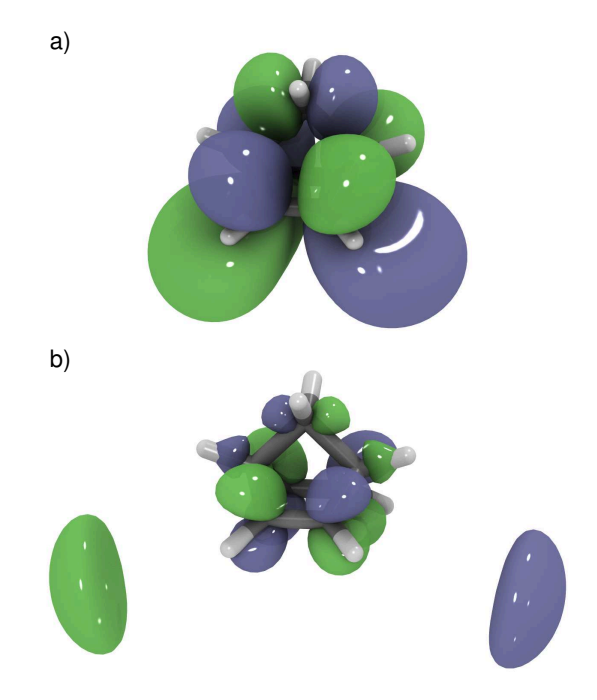


FIG. 10. a) Real and b) imaginary parts of the normalized Dyson orbital connected with the 2B_2 (π_+^*) shape resonance of the norbornadiene anion computed at the EA-ADC(2)/TZ level of theory. Isosurfaces were drawn at function values of ± 0.0175 (real part) and ± 0.0065 (imaginary part).

being 0.625/0.329 (2A_2) and 0.802/0.124 (2B_2). The Dyson orbital of the π_+^* combination (2B_2) shows that even though the CH-units cannot mediate a significant through-bond interaction, the bridging methylene moiety is able to do so. Moreover, owing to the puckered ring, a direct through-space interaction is possible as suggested by the extended lobes of the Dyson orbitals.

The computed resonance parameters of norbornadiene are collected in Table IV. Both positions agree amazingly well with the experimental ETS values. ⁶⁸ Our calculations thus confirm that the π^* resonances follow the expected natural ordering. The resonance position of the π_+^* (²B₂) state predicted by CAP/EA-ADC(2)/TZ is $E_r = 0.955$ eV, considerably lower than that of the π_-^* (²A₂) state: $E_r = 2.586$ eV. Regarding the widths,

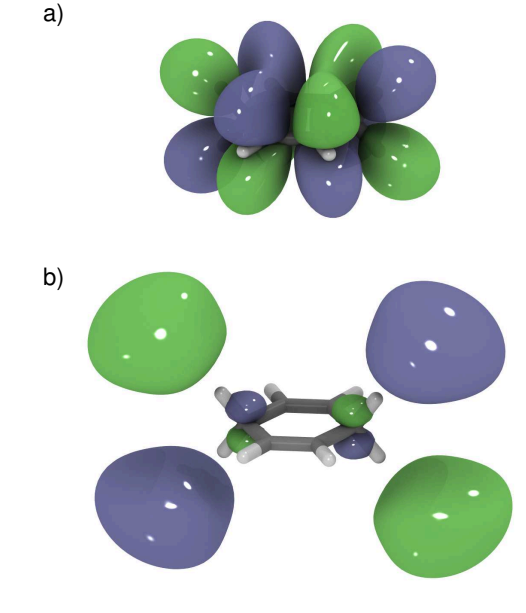


FIG. 11. a) Real and b) imaginary parts of the normalized Dyson orbital connected with the $^2B_{2g}$ (π_+^*) shape resonance of the 1,4-cyclohexadiene anion computed at the EA-ADC(2)/TZ level of theory. Isosurfaces were drawn at function values of ± 0.0175 (real part) and ± 0.0040 (imaginary part).

CAP/EA-ADC yields higher values for the 2A_2 state than for the 2B_2 state. Although no definite experimental data is available in this case, this trend is consistent with the shape of the recorded electron transmission spectrum, 68 where a broader peak is observed for the higher-lying spectral feature (see Figure 8).

We now turn to 1,4-cyclohexadiene. Its two π^* resonances show $^2B_{2g}$ and 2A_u symmetry, and the Dyson orbitals associated with these two states as calculated at the CAP/EA-ADC(2)/TZ level of theory are displayed in Figures 11 and 12, respectively. As for norbornadiene, both considered attachment processes are characterized by a predominant one-electron character, as suggest the weights of the Dyson orbitals of 0.922 ($^2B_{2g}$) and 0.914 (2A_u). In this case, the relative weights of the real/imaginary parts are 0.880/0.042 ($^2B_{2g}$) and

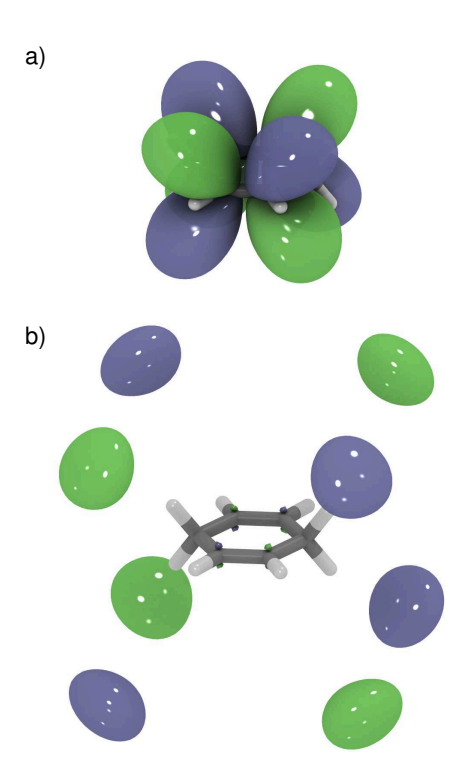


FIG. 12. a) Real and b) imaginary parts of the normalized Dyson orbital corresponding to the 2A_u (π^*_-) shape resonance of the 1,4-cyclohexadiene anion computed at the EA-ADC(2)/TZ level of theory. Isosurfaces were drawn at function values of ± 0.0175 (real part) and ± 0.0038 (imaginary part).

0.877/0.036 (2A_u). As expected, for 1,4-cyclohexadiene the energetic order of the resonance states is reversed. Here, the π_+^* ($^2B_{2g}$) state is strongly affected by throughbond interactions, and one additional nodal plane appears due to the interaction with the π -like CH- σ combinations at the methylene moieties. By contrast, the antisymmetric π_-^* combination (2A_u) is simply a mixture of the two ethylenic π^* orbitals.

The computed resonance positions and decay widths of 1.4-cyclohexadiene are summarized in Table V. Again. the agreement with the experimental resonance positions is excellent: for the $^2\mathrm{B}_{2\mathrm{g}}$ (π_+^*) state the computed position is 2.651 eV while the experimental value is 2.67 eV, and for the ${}^{2}A_{u}$ (π_{-}^{*}) state the computed position is $E_r = 1.735 \text{ eV}$ while the experimental value is 1.75 eV.⁶⁸ Thus, again, the CAP/EA-ADC(2)/TZ calculations confirm the expected energetic order with a lower π_{-}^{*} state for through-bond systems. Regarding widths, as for norbornadiene, vibrational bands were not resolved in the ETS experiment, and a direct comparison with the computed width is not possible. However, the recorded spectrum reveals considerably narrower bands than those observed in the norbornadiene spectrum (Figure 8) suggesting narrower widths, and this trend is confirmed by the calculated CAP/EA-ADC widths.

V. SUMMARY AND CONCLUSIONS

An in-depth investigation of various theoretical and conceptual aspects of our recently introduced subspace-projected CAP/EA-ADC method has been presented. For this purpose, our guinea pig is the well-studied $^2\Pi_{\rm g}$ resonance of the dinitrogen anion N_2^- . We study, in particular, the problem of the choice of the subspace used to represent the CAP. As a rule of thumb, the subspace may be composed using an energy criterion, i.e., electronic states within a range of a few resonance widths around the expected resonance position should be included. In case of the $^2\Pi_{\rm g}$ resonance of N_2^- , for example, a subspace composed of all states within ± 5 eV around the resonance position was found to be sufficient to achieve satisfactory results.

All considered CAP/EA-ADC schemes were shown to provide satisfactory results. The resonance positions computed using EA-ADC(2) and standard EA-ADC(3) are in excellent agreement with the experimental values. The corresponding resonance width is best reproduced by strict EA-ADC(3), but also standard EA-ADC(3) and EA-ADC(2) perform reasonably well. Furthermore, we extended the methodology to complex potential strengths. However, only a slight improvement of the resonance parameters computed using standard EA-ADC(3) was observed.

In order to further investigate the performance of CAP/EA-ADC, we applied the methodology to π^* resonances of unsaturated hydrocarbons. Using ethylene as a prototype for this class of molecules, the same behavior as for the $^2\Pi_{\rm g}$ resonance of ${\rm N}_2^-$ was observed: The resonance position is best reproduced by CAP/EA-ADC(2) using a triple-zeta basis set whereas CAP/EA-ADC(3) provides the best resonance widths. However, all employed EA-ADC schemes yield satisfactory results.

By applying our CAP/EA-ADC methods to the π_{\perp}^* and π_{-}^{*} resonances of the anions of the medium-sized organic dienes norbornadiene and 1,4-cyclohexadiene, the first many-body treatment of these systems is provided. The same performance of CAP/EA-ADC(2) as seen for N_2^- and ethylene was observed also for these systems. The experimentally determined resonance positions are perfectly reproduced when a diffuse triple-zeta basis set is employed. Because of the lack of vibrational resolution in the experimental electron transmission spectra, no direct comparison of the computed widths with experimental values is possible. However, the computed values are generally consistent with the spectral shape, i.e., in case of the norbornadiene anion, a larger width was found for the ${}^{2}A_{2}$ (π_{-}^{*}) resonance than for the ${}^{2}B_{2}$ (π_{+}^{*}) one. Similarly, for both the $^2\mathrm{B}_{2\mathrm{g}}$ (π_+^*) and $^2\mathrm{A}_\mathrm{u}$ (π_-^*) resonances of the 1,4-cyclohexadiene anion, the computed widths are smaller than for the respective resonance states of the norbornadiene anion, again being consistent with the shape of the recorded experimental spectra.

Our results also confirm the order of the π^* resonances in these diene systems. In case of norbornadi-

TABLE V. Resonance parameters of the $^2B_{2g}$ and 2A_u anionic shape resonances of 1,4-cyclohexadiene as extracted from the corrected trajectories computed using different EA-ADC schemes and employing double-zeta (DZ) and triple-zeta (TZ) basis sets as specified in Section III. The experimentally determined resonance positions are $E_r(^2B_{2g}) = 2.67$ eV and $E_r(^2A_u) = 1.75$ eV.

-	DZ				TZ			
State	EA-ADC scheme	$E_r [eV]$	$\Gamma [\mathrm{eV}]$	$\eta_{ m opt}$	$E_r [eV]$	$\Gamma \left[\mathrm{eV} \right]$	$\eta_{ m opt}$	
$^{2}\mathrm{B}_{2\mathrm{g}}~(\pi_{+}^{*})$	EA-ADC(2)	2.922	0.096	1.97×10^{-3}	2.651	0.078	1.37×10^{-3}	
	Strict EA-ADC (3)	3.253	0.163	2.00×10^{-3}	3.185	0.229	1.63×10^{-3}	
	Standard EA-ADC(3)	3.203	0.147	1.98×10^{-3}	3.091	0.177	1.54×10^{-3}	
$^{2}A_{u}(\pi_{-}^{*})$	EA-ADC(2)	1.974	0.178	1.24×10^{-3}	1.735	0.127	8.64×10^{-4}	
	Strict EA-ADC (3)	2.359	0.232	4.77×10^{-3}	2.289	0.240	3.35×10^{-3}	
	Standard EA-ADC(3)	2.311	0.215	4.80×10^{-3}	2.203	0.205	3.35×10^{-3}	

ene, the π_+^* (2B_2) resonance appears at lower energy than the π_-^* combination 2A_2 , showing the expected energetic ordering of the π^* orbitals implied by predominant through-space interaction. On the contrary, a reversed energetic ordering of the π^* orbitals is observed for 1,4-cyclohexadiene. Owing to through-bond interactions of the ethylenic π^* orbitals with suitable linear combinations of the occupied C-H σ orbitals at the methylene moieties, the π_+^* combination is pushed above the π_-^* combination. As a result, the π_+^* ($^2B_{2g}$) resonance is found at a considerably higher energy than the π_-^* (2A_u) resonance.

In conclusion, CAP/EA-ADC methods can be considered reliable and computationally cost-efficient tools for the description of electronic resonances. Especially the good performance of CAP/EA-ADC(2) invites the study of shape resonances in larger molecular systems.

SUPPLEMENTARY MATERIAL

See supplementary material for molecular geometries of all studied compounds and plots of CAP trajectories.

ACKNOWLEDGMENTS

A.L.D. acknowledges financial support by the Research Unit "Intermolecular and Interatomic Coulombic Decay" (FOR 1789) funded by the German Research Foundation. A.M.B. acknowledges Grant No. 19-33-90213 from the Russian Foundation for Basic Research and thanks the Irkutsk Supercomputer Center of SB RAS for providing computational resources of the HPC-cluster "Akademik V.M. Matrosov". T.S. gratefully acknowledges support from the National Science Foundation under Grant No. 1856775. A.B.T. acknowledges support from the Ministry of Science and Higher Education of the Russian Federation (Grant No. FZZE-2020-0025). We dedicate this paper to Prof. Dr. Rolf Gleiter on the occasion of his 85th birthday.

DATA AVAILABILITY

The data that supports the findings of this study are available within the article and its supplementary material. Additional data are available from the corresponding author upon reasonable request.

- ¹M. C. Boyer, N. Rivas, A. A. Tran, C. A. Verish, and C. R. Arumainayagam, Surf. Sci. 652, 26 (2016).
- ²E. Böhler, J. Warneke, and P. Swiderek, Chem. Soc. Rev. 42, 9219 (2013).
- ³E. Alizadeh, T. M. Orlando, and L. Sanche, Annu. Rev. Phys. Chem. **66**, 379 (2015).
- ⁴I. Bald, R. Čurík, J. Kopyra, and M. Tarana, "Dissociative electron attachment to biomolecules," in *Nanoscale Insights into Ion-Beam Cancer Therapy*, edited by A. V. Solov'yov (Springer International Publishing, Cham, 2017) pp. 159–207.
- ⁵R. Santra and L. S. Cederbaum, Phys. Rep. **368**, 1 (2002).
- ⁶T.-C. Jagau, K. B. Bravaya, and A. I. Krylov, Annu. Rev. Phys. Chem. **68**, 525 (2017).
- ⁷A. J. F. Siegert, Phys. Rev. **56**, 750 (1939).
- ⁸J. M. Herbert, "The quantum chemistry of loosely-bound electrons," in *Reviews in Computational Chemistry Volume 28* (John Wiley & Sons, Ltd, 2015) Chap. 8, pp. 391–517.
- ⁹K. D. Jordan and P. D. Burrow, Acc. Chem. Res **11**, 341 (1978).
 ¹⁰V. Balaji, L. Ng, K. D. Jordan, M. N. Paddon-Row, and H. K. Patney, J. Am. Chem. Soc. **109**, 6957 (1987).
- ¹¹K. D. Jordan and P. D. Burrow, Chemical Reviews 87, 557 (1987).
- ¹²M. Allan and L. Andric, J. Chem. Phys. **105**, 3559 (1996).
- ¹³U. V. Riss and H.-D. Meyer, J. Phys. B: At. Mol. Opt. Phys. **26**, 4503 (1993).
- ¹⁴U. V. Riss and H.-D. Meyer, J. Chem. Phys. **105**, 1409 (1996).
- ¹⁵U. V. Riss and H.-D. Meyer, J. Phys. B: At. Mol. Opt. Phys. **31**, 2279 (1998).
- ¹⁶S. Kopelke, K. Gokhberg, V. Averbukh, F. Tarantelli, and L. S. Cederbaum, J. Chem. Phys. **134**, 094107 (2011).
- ¹⁷N. Moiseyev, Non-Hermitian Quantum Mechanics (Cambridge University Press, 2011).
- ¹⁸J. D. Morgan and B. Simon, J. Phys. B: At. Mol. Phys. **14**, L167 (1981).
- ¹⁹N. Moiseyev, Phys. Rep. **302**, 212 (1998)
- $^{20}{\rm B.~Simon,~Phys.~Lett.~A}$ **71**, 211 (1979).
- ²¹C. W. McCurdy and T. N. Rescigno, Phys. Rev. Lett. **41**, 1364 (1978).
- ²²W. P. Reinhardt, Annu. Rev. Phys. Chem. **33**, 223 (1982).
- ²³A. F. White, M. Head-Gordon, and C. W. McCurdy, J. Chem. Phys. **142**, 054103 (2015).
- ²⁴T. Sommerfeld, U. V. Riss, H.-D. Meyer, L. S. Cederbaum, B. Engels, and H. U. Suter, J. Phys. B: At. Mol. Opt. Phys. 31, 4107 (1998).

²⁵T. Sommerfeld and R. Santra, Int. J. Quantum Chem. **82**, 218 (2001).

- ²⁶R. Santra and L. S. Cederbaum, J. Chem. Phys. **117**, 5511 (2002).
- ²⁷S. Feuerbacher, T. Sommerfeld, R. Santra, and L. S. Cederbaum,
 J. Chem. Phys. 118, 6188 (2003).
- ²⁸Y. Sajeev, R. Santra, and S. Pal, J. Chem. Phys. **122**, 234320 (2005).
- ²⁹N. Vaval and L. S. Cederbaum, J. Chem. Phys. **126**, 164110 (2007).
- ³⁰M. Ehara and T. Sommerfeld, Chem. Phys. Lett. **537**, 107 (2012).
- ³¹Y. Zhou and M. Ernzerhof, J. Phys. Chem. Lett. 3, 1916 (2012).
 ³²A. Ghosh, N. Vaval, and S. Pal, J. Chem. Phys. 136, 234110 (2012).
- ³³T.-C. Jagau and A. I. Krylov, J. Phys. Chem. Lett. 5, 3078 (2014).
- ³⁴A. A. Kunitsa, A. A. Granovsky, and K. B. Bravaya, J. Chem. Phys. **146**, 184107 (2017).
- ³⁵Q. M. Phung, Y. Komori, T. Yanai, T. Sommerfeld, and M. Ehara, J. Chem. Theory Comput. 16, 2606 (2020).
- ³⁶S. Das, Y. Sajeev, and K. Samanta, J. Chem. Theory Comput. 16, 5024 (2020).
- ³⁷S. Basumallick, S. Bhattacharya, I. Jana, N. Vaval, and S. Pal, Mol. Phys. **118**, e1726521 (2020).
- ³⁸ A. M. Belogolova, A. L. Dempwolff, A. Dreuw, and A. B. Trofimov, J. Phys. Conf. Ser. **1847**, 012050 (2021).
- ³⁹ J. Schirmer, A. B. Trofimov, and G. Stelter, J. Chem. Phys. 109, 4734 (1998).
- ⁴⁰A. B. Trofimov and J. Schirmer, J. Chem. Phys. **123**, 144115 (2005).
- ⁴¹A. L. Dempwolff, A. M. Belogolova, A. B. Trofimov, and A. Dreuw, J. Chem. Phys. **154**, 104117 (2021).
- ⁴²A. L. Dempwolff, M. Schneider, M. Hodecker, and A. Dreuw, J. Chem. Phys. **150**, 064108 (2019).
- ⁴³ A. L. Dempwolff, A. C. Paul, A. M. Belogolova, A. B. Trofimov, and A. Dreuw, J. Chem. Phys. **152**, 024113 (2020).
- ⁴⁴A. L. Dempwolff, A. C. Paul, A. M. Belogolova, A. B. Trofimov, and A. Dreuw, J. Chem. Phys. **152**, 024125 (2020).
- $^{45}{\rm J}.$ Schirmer, Phys. Rev. A ${\bf 26},\,2395$ (1982).
- ⁴⁶A. B. Trofimov, G. Stelter, and J. Schirmer, J. Chem. Phys. 117, 6402 (2002).
- ⁴⁷J. Schirmer and A. B. Trofimov, J. Chem. Phys. **120**, 11449 (2004).
- ⁴⁸A. Dreuw and M. Wormit, WIREs Comput. Mol. Sci. 5, 82 (2015).
- ⁴⁹A. Dreuw, "The algebraic-diagrammatic construction scheme for the polarization propagator," in *Quantum Chemistry and Dynamics of Excited States* (John Wiley & Sons, Ltd, 2020) Chap. 5, pp. 109–131.
- ⁵⁰M. Wormit, D. R. Rehn, P. H. P. Harbach, J. Wenzel, C. M. Krauter, E. Epifanovsky, and A. Dreuw, Mol. Phys. **112**, 774 (2014).
- ⁵¹P. H. P. Harbach, M. Wormit, and A. Dreuw, J. Chem. Phys. 141, 064113 (2014).
- ⁵²E. Épifanovsky, A. T. B. Gilbert, X. Feng, J. Lee, Y. Mao, N. Mardirossian, P. Pokhilko, A. F. White, M. P. Coons, A. L. Dempwolff, Z. Gan, D. Hait, P. R. Horn, L. D. Jacobson, I. Kaliman, J. Kussmann, A. W. Lange, K. U. Lao, D. S. Levine, J. Liu, S. C. McKenzie, A. F. Morrison, K. D. Nanda, F. Plasser, D. R. Rehn, M. L. Vidal, Z.-Q. You, Y. Zhu, B. Alam, B. J. Albrecht, A. Aldossary, E. Alguire, J. H. Andersen, V. Athavale, D. Barton, K. Begam, A. Behn, N. Bellonzi, Y. A. Bernard, E. J. Berquist, H. G. A. Burton, A. Carreras, K. Carter-Fenk, R. Chakraborty, A. D. Chien, K. D. Closser, V. Cofer-Shabica, S. Dasgupta, M. de Wergifosse, J. Deng, M. Diedenhofen, H. Do, S. Ehlert, P.-T. Fang, S. Fatehi, Q. Feng, T. Friedhoff, J. Gayvert, Q. Ge, G. Gidofalvi, M. Goldey, J. Gomes, C. E. González-Espinoza, S. Gulania, A. O. Gunina, M. W. D. Hanson-Heine, P. H. P. Harbach,

A. Hauser, M. F. Herbst, M. Hernández Vera, M. Hodecker, Z. C. Holden, S. Houck, X. Huang, K. Hui, B. C. Huynh, M. Ivanov, Á. Jász, H. Ji, H. Jiang, B. Kaduk, S. Kähler, K. Khistyaev, J. Kim, G. Kis, P. Klunzinger, Z. Koczor-Benda, J. H. Koh, D. Kosenkov, L. Koulias, T. Kowalczyk, C. M. Krauter, K. Kue, A. Kunitsa, T. Kuś, I. Ladjánszki, A. Landau, K. V. Lawler, D. Lefrancois, S. Lehtola, R. R. Li, Y.-P. Li, J. Liang, M. Liebenthal, H.-H. Lin, Y.-S. Lin, F. Liu, K.-Y. Liu, M. Loipersberger, A. Luenser, A. Manjanath, P. Manohar, E. Mansoor, S. F. Manzer, S.-P. Mao, A. V. Marenich, T. Markovich, S. Mason, S. A. Maurer, P. F. McLaughlin, M. F. S. J. Menger, J.-M. Mewes, S. Mewes, P. Morgante, J. W. Mullinax, K. J. Oosterbaan, G. Paran, A. C. Paul, S. K. Paul, F. Pavošević, Z. Pei, S. Prager, E. I. Proynov, A. Rák, E. Ramos-Cordoba, B. Rana, A. E. Rask, A. Rettig, R. M. Richards, F. Rob, E. Rossomme, T. Scheele, M. Scheurer, M. Schneider, N. Sergueev, S. M. Sharada, W. Skomorowski, D. W. Small, C. J. Stein, Y.-C. Su, E. J. Sundstrom, Z. Tao, J. Thirman, G. J. Tornai, T. Tsuchimochi, N. M. Tubman, S. P. Veccham, O. Vydrov, J. Wenzel, J. Witte, A. Yamada, K. Yao, S. Yeganeh, S. R. Yost, A. Zech, I. Y. Zhang, X. Zhang, Y. Zhang, D. Zuev, A. Aspuru-Guzik, A. T. Bell, N. A. Besley, K. B. Bravaya, B. R. Brooks, D. Casanova, J.-D. Chai, S. Coriani, C. Cramer, G. Cserey, A. E. DePrince III, R. A. DiStasio Jr., A. Dreuw, B. D. Dunietz, T. R. Furlani, W. A. Goddard III, S. Hammes-Schiffer, T. Head-Gordon, W. J. Hehre, C.-P. Hsu, T.-C. Jagau, Y. Jung, A. Klamt, J. Kong, D. S. Lambrecht, W. Liang, N. J. Mayhall, C. W. Mc-Curdy, J. B. Neaton, C. Ochsenfeld, J. A. Parkhill, R. Peverati, V. A. Rassolov, Y. Shao, L. V. Slipchenko, T. Stauch, R. P. Steele, J. E. Subotnik, A. J. W. Thom, A. Tkatchenko, D. G. Truhlar, T. Van Voorhis, T. A. Wesolowski, K. B. Whaley, H. L. Woodcock III, P. M. Zimmerman, S. Faraji, P. M. W. Gill, M. Head-Gordon, J. M. Herbert, and A. I. Krylov, J. Chem. Phys. (2021), 10.1063/5.0055522.

- ⁵³T. Sommerfeld and M. Ehara, J. Chem. Theory Comput. 11, 4627 (2015).
- ⁵⁴J. Schirmer, Phys. Rev. A **43**, 4647 (1991).
- ⁵⁵V. Weisskopf and E. Wigner, Z. Phys. **63**, 54 (1930).
- ⁵⁶U. Fano, Phys. Rev. **124**, 1866 (1961).
- ⁵⁷H. Feshbach, Ann. Phys. (N.Y.) **5**, 357 (1958).
- ⁵⁸H. Feshbach, Ann. Phys. (N.Y.) **19**, 287 (1962).
- $^{59}{\rm T.-C.}$ Jagau and A. I. Krylov, J. Chem. Phys. ${\bf 144},054113$ (2016). $^{60}{\rm T.}$ H. Dunning, J. Chem. Phys. ${\bf 90},$ 1007 (1989).
- ⁶¹R. A. Kendall, T. H. Dunning, and R. J. Harrison, J. Chem. Phys. **96**, 6796 (1992).
- ⁶²W. Humphrey, A. Dalke, and K. Schulten, J. Molec. Graphics 14, 33 (1996).
- ⁶³R. Hoffmann, E. Heilbronner, and R. Gleiter, J. Am. Chem. Soc. 92, 706 (1970).
- ⁶⁴R. Hoffmann, Acc. Chem. Res **4**, 1 (1971).
- ⁶⁵D. Zuev, T.-C. Jagau, K. B. Bravaya, E. Epifanovsky, Y. Shao, E. Sundstrom, M. Head-Gordon, and A. I. Krylov, J. Chem. Phys. **141**, 024102 (2014).
- ⁶⁶M. Berman, H. Estrada, L. S. Cederbaum, and W. Domcke, Phys. Rev. A 28, 1363 (1983).
- ⁶⁷R. Panajotovic, M. Kitajima, H. Tanaka, M. Jelisavcic, J. Lower, L. Campbell, M. J. Brunger, and S. J. Buckman, J. Phys. B: At. Mol. Opt. Phys. 36, 1615 (2003).
- ⁶⁸K. D. Jordan, J. A. Michejda, and P. D. Burrow, Chem. Phys. Lett. **42**, 227 (1976).
- ⁶⁹R. McDiarmid and J. P. Doering, J. Chem. Phys. **75**, 2687 (1981).
 ⁷⁰A. Modelli, D. Jones, S. Rossini, and G. Distefano, Chem. Phys. Lett. **123**, 375 (1986).
- ⁷¹M. F. Falcetta and K. D. Jordan, J. Am. Chem. Soc. **113**, 2903 (1991).
- ⁷²C.-Y. Juang and J. S.-Y. Chao, J. Phys. Chem. **98**, 13506 (1994).